CONF-760716--4

b.c.c. TRANSITION METALS UNDER PRESSURE: RESULTS FROM ULTRASONIC INTERFEROMETRY AND DIAMOND-CELL EXPERIMENTS

K. W. Katahara, M. H. Manghnani,
L. C. Ming and E. S. Fisher

U. S. - Japan Seminar on "High-pressure
Research Applications in Geophysics"
Honolulu, Hawaii
July 6-9, 1976

ARGONNE NATIONAL LABORATORY, ARGONNE, ILLINOIS

Operated for the U. S. ENERGY RESEARCH
AND DEVELOPMENT ADMINISTRATION
under Contract W-31-109-Eng-38

b.c.c. TRANSITION METALS UNDER PRESSURE: RESULTS FROM ULTRASONIC INTERFEROMETRY AND DIAMOND-CELL EXPERIMENTS

by

K. W. Katahara, M. H. Manghnani, and L. C. Ming

Hawaii Institute of Geophysics
University of Hawaii
Honolulu, Hawaii 96822

and

E. S. Fisher

Argonne National Laboratory
Argonne, Illinois 60439

August 1976

Submitted for publication in the *Proceedings of the U.S.-Japan Seminar on High-pressure Research Applications in Geophysics*, July 6-9, 1976, Honolulu, Hawaii.

b.c.c. TRANSITION METALS UNDER PRESSURE: RESULTS FROM ULTRASONIC INTERFEROMETRY AND DIAMOND-CELL EXPERIMENTS

by

K. W. Katahara, M. H. Manghnani, and L. C. Ming
Hawaii Institute of Geophysics
University of Hawaii
Honolulu, Hawaii 96822

and

E. S. Fisher
Argonne National Laboratory
Argonne, Illinois

ABSTRACT

Hydrostatic pressure derivatives of the single-crystal elastic moduli, dC_{ij}/dP, have been measured ultrasonically for b.c.c. niobium-molybdenum and tantalum-tungsten solid solutions. The composition dependence of various electronic properties of these alloys is known to be reasonably well approximated by a rigid-electron-band filling model where e/a, the electron per atom ratio, is the primary parameter. The results indicate that the elastic moduli and their pressure derivatives may also be calculated in such a model. In particular, the dC_{ij}/dP show relatively sharp increases at e/a compositions of 5.4 for Nb-Mo and 5.7 for Ta-W. Both compositions correspond to changes in Fermi surface topology, as deduced from existing band calculations and the rigid band assumption. The results are discussed in the light of related electronic properties and possible geophysical applications.

A comparison is also made between ultrasonic results and X-ray diffraction data for Nb. Using diamond-anvil pressure cell, compression of Nb was determined by X-ray diffraction up to 55 kbar in a liquid medium under purely hydrostatic conditions, and up to 175 kbar in a solid medium under nonhydrostatic conditions. The data obtained under hydrostatic conditions agree well with the ultrasonic equation of state and shock wave data, whereas the nonhydrostatic results tend to imply either a higher bulk modulus K_S or a higher $(\partial K_S/\partial P)_T$.

INTRODUCTION

Band structure calculations have recently been used to study the elastic properties of geophysically important materials [Thomsen, 1975; Bukowinski and Knopoff, 1976, and in this volume]. In particular, Bukowinski and Knopoff [1976 and in this volume] have evaluated the density and bulk modulus of iron at core pressures. Another step along these lines would be to compute the shear elastic moduli of highly compressed iron in order to compare them with seismic values for the inner core as obtained, for instance, by Gilbert and Dziewonski [1975] or Anderson and Hart [1976]. Unfortunately, efficient theoretical methods have not yet been developed for calculating shear moduli in transition metals, and it is only recently that attempts have been made in this direction [e.g., Oli and Animalu, 1976; Peter et al., 1974]. The research reported here may be regarded as an experimental approach to this problem. The elastic moduli, C_{ij}, and their pressure derivatives, dC_{ij}/dP, have been measured ultrasonically for single crystal Nb-Mo and Ta-W alloys. The results for these materials are in some respects ideal for testing and refining any theoretical methods which might be applied to calculating the shear moduli of iron at core pressures.

The electronic band structures of the transition metals are characterized by narrow d-electron bands crossing and hybridizing with a broader nearly-free electron band, and the properties of these metals are largely dominated by the behavior of the electrons in the d-bands. The bcc transition metals of

groups VB (V, Nb, Ta) and VIB (Cr, Mo, W) have particularly strong band structure contributions to the cohesive energy [Pettifor, 1970], the elastic moduli [Fisher, 1973], and the pressure derivative of the bulk modulus [Fisher et al., 1975]. Thus any theoretical models which can successfully explain the present results might be expected to be applicable to other transition metals where d-band effects are not as pronounced.

Another useful property of the bcc transition metals is that they form randomly disordered solid solutions over a wide range of compositions so that the population of electrons in the bands can be varied at constant crystal structure and slowly varying atomic volume. In the following, the alloy compositions will be characterized by the e/a ratio, defined as the average number of conduction electrons per atom, which is 5 and 6 for the group VB and VIB elements respectively. At atmospheric pressure and room temperature these elements form bcc alloys with each other and with elements of groups IVB and VIIB (and VIII to some extent) over the e/a range shown in Table 1 [Pearson, 1958, 1966]. The stability of the bcc structure over a wide e/a range becomes useful when it is recognized that the rigid band model works reasonably well for these metals, as shown by comparisons between experimental and theoretical densities of states [McMillan, 1968; Pickett and Allen, 1974]. The rigid band model is here intended not to include the assumption, which is known to fail [Posternak et al., 1975], that the bands remain rigid when the lattice is deformed. Rather, it is only

assumed that within the Brillouin zone of the lattice, which may be either deformed or undeformed, the shapes of the bands do not change very much as an element is alloyed with neighboring elements. Thus by varying the alloy composition, and hence changing e/a and the Fermi energy, E_F, the properties of different energy regions of the electronic band structure can be experimentally examined. A theoretical calculation of the strain derivatives of the electronic energy levels would then need to be done for only one bcc element of group VB or VIB, and the results for its solid solutions could be obtained by adding or subtracting electrons. Any valid calculational scheme should thus be capable of at least qualitatively reproducing the present results.

Some of the more interesting aspects of these results and their connection with the electronic band structure are discussed in the next section. A more complete discussion, together with a description of the samples and the experimental details, will be published elsewhere [Katahara et al., in preparation].

The last section of this paper is concerned with the accuracy of the present ultrasonic measurements and of diamond-anvil compression studies. Equations of state obtained by different methods for the pure elements are compared and the sources of disagreement are discussed.

RESULTS AND DISCUSSION FOR THE SOLID SOLUTIONS

The adiabatic single crystal C_{ij} and dC_{ij}/dP were measured ultrasonically for 6 Nb-Mo alloys, 5 Ta-W alloys and the pure elements Mo and W. The experimental methods have been described in a previous paper [Katahara et al., 1976] in which data on the other two end members, Nb and Ta, were reported.

Figures 1 and 2 show the present C_{ij} values for the alloys together with the previous results of Hubbell and Brotzen [1972] for the Nb-Mo system, and the unpublished results of Shannette [personal communication] on some rather inhomogeneous Ta-W solid solutions. $C_L = (C_{11} + C_{12})/2 + C_{44}$ is the effective elastic coefficient for longitudinal waves propagating along [110], K_s is the adiabatic bulk modulus, and $C' = (C_{11} - C_{12})/2$ is the effective elastic coefficient for shear waves propagating along [110] and polarized along $[1\bar{1}0]$. Note that the bulk modulus increases nearly linearly with e/a (as does the density [see Pearson, 1966, and references given there]). The shear moduli, C_{44} and C', and the longitudinal moduli C_{11} and C_L, show more structure in their e/a dependence, and this is more so for C_{44} and C_L than for C' and C_{11}. Since longitudinal strains include both shear and volume components, it is clear that it is the response of the electrons to shear that is causing the marked variation of these moduli with e/a. In the following, the main emphasis will therefore be on the shear moduli. These quantities increase slowly at first for low e/a, then they begin to increase more rapidly with the curves reaching inflection points at

e/a ∿ 5.4 for the Nb-Mo alloys and at e/a ∿ 5.7 for the Ta-W alloys.

As discussed extensively by Fisher [1973] simple, nearly free-electron metals crystallizing in the b.c.c. structure generally have C_{44} much greater than C'. In Figure 1 we see that the opposite occurs for the Nb-Mo alloys indicating strong band structure effects on the shear moduli. On the other hand, C_{44} is either greater or slightly less than C' in Figure 2. This is interpreted to mean that the Ta-W alloys are in a sense more free-electron-like than the Nb-Mo alloys. In fact, the 5d-bands in Ta are broader than the 4d-bands in Nb [Mattheiss, 1970] indicating less localization of the conduction electrons in the Ta-W alloys.

Figures 3 and 4 show the dC_{ij}/dP for the Nb-Mo and Ta-W alloys respectively. The dK_s/dP values, like the bulk moduli themselves, vary relatively smoothly with e/a as compared to the pressure derivatives of the shear moduli. For both the solid solution systems, dC_{44}/dP and dC'/dP at first increase slowly near e/a ∿ 5, then increase more radpily after which the curves level out rather abruptly. These trends are enhanced in the plots of $\pi_{ij} = d \ln C_{ij}/d \ln V$ vs. e/a in Figures 5 and 6. The pronounced extrema for the Nb-Mo alloys appear at e/a = 5.4 (Fig. 5). The extrema for the T-W alloys seem to be broader and are located near e/a ∿ 5.7 (Fig. 6); but the broadness and position are rather uncertain because there was only one alloy with a composition in the region of interest.

In Figure 7 ℓn A (where $A = C_{44}/C'$) and d ℓn A/d ℓn V are shown as functions of e/a. We note the sharp minimum in d ℓn A/d ℓn V at e/a = 5.4 for the Nb-Mo system, and the broad minimum at e/a ∿ 5.7 for the Ta-W system.

Some of the features of the preceding results can be correlated with the band structure. A sketch of the energy bands along [100] in reciprocal space is shown in Figure 8. Γ is the center of the Brillouin zone and H is a corner along [100]. This figure has been adapted from the tungsten band structure of Mattheiss [1965], but all of the bcc transition metals have very similar band structures. The broken lines indicate roughly the Fermi energies corresponding to e/a values of 5 and 6. Concentrating for the moment on the left side of the figure, note that as e/a increases from 5 to 6, E_F passes through the level Γ_{25}' where the Fermi surface topology changes. Mattheiss [1970] has calculated band structures and densities of states for Nb and Ta. From his Figure 3 and the rigid band assumption discussed earlier, it is estimated that Γ_{25}' is just occupied at e/a ∿ 5.4 for the Nb-Mo alloys and e/a ∿ 5.7 for the Ta-W alloys. These are the e/a values at which the inflection points in the C_{ij} and the extrema in the π_{ij} are observed. It thus appears that the energy levels near Γ_{25}' contribute strongly to the shear moduli and their pressure derivatives. The relative broadness of the extrema for the Ta-W π_{ij} and d ℓn A/d ℓn V may be partly due to spin-orbit splitting which is much stronger in the 5d elements. This is illustrated on the right hand side of Figure 8.

The point Γ_{25}', which is triply degenerate, is split and the result may be to smear out the effects on the shear moduli.

Although it is possible to qualitatively correlate the results of this study with the band structure, a fundamental explanation of how shear strains affect the electronic energy levels requires the framework of a theoretical model. It is hoped that the present results will both stimulate and provide a good test for further theoretical work in this direction.

The present study also illustrates a point possibly applicable to the earth's core: that relatively small changes in e/a can lead to large changes in transition metal properties. This has been shown here for the shear moduli and their pressure derivatives. Another quantity that may have important geophysical implication is the electronic Grüneisen parameter,

$$\gamma_e = \frac{d \ \ell n \ N(E_F)}{d \ \ell n \ V}$$

where $N(E_F)$ is the density of states at the Fermi energy. Smith and Finlayson [1976] have demonstrated that for the bcc transition metals γ_e varies appreciably with e/a. One might therefore speculate that these properties will also vary rapidly with e/a for iron solid solutions in the core. If, for instance, a small amount of sulfur were dissolved in iron at core pressures, the iron conduction bands would presumably be distorted slightly, but the major effect might well be due to the creation, and filling, of sulfur 3p bands below the conduction bands. The

c/a ratio would be decreased and the shear moduli, γ_c, and other properties could be substantially different from those calculated for pure iron.

EQUATIONS OF STATE

A problem that frequently arises in equation of state studies is that P-V measurements by different methods, or by different workers using the same method, do not agree. Figures 9 and 10 illustrate this point for the metals of groups VB (Nb and Ta) and VIB (Mo and W), respectively. The curves shown are a) the shock Hugoniots of McQueen at al. [1970] centered at 20°C and zero pressure, b) 20°C isotherms obtained by McQueen et al. [1970] from the Hugoniots, and c) 25°C isotherms extrapolated from the ultrasonic measurements of the present study and of Katahara et al. [1976] according to the Birch-Murnaghan equation [Birch, 1938, 1947]:

$$P = \frac{3}{2} K_T \left[\left(\frac{V_o}{V} \right)^{7/3} - \left(\frac{V_o}{V} \right)^{5/3} \right] \left\{ 1 - \frac{3}{4} (4 - K_T') \right.$$

$$\left. \times \left[\left(\frac{V_o}{V} \right)^{2/3} - 1 \right] + \ldots \right\} \qquad (1)$$

Here K_T, the isothermal bulk modulus, and $K_T' = (\partial K_T / \partial P)_T$, have been derived from the corresponding adiabatic values, measured ultrasonically, according to equation 10.15 of Thurston [1965,

p. 1331]. Terms in (1) involving second and higher order derivatives of the bulk modulus have been neglected.

Note that the ultrasonic isotherms give uniformly higher volumes than the shock compression isotherms. This is not unexpected because errors in the ultrasonic measurements due to densification of the presence medium [Katahara et al., 1976] and to transducer and bond effects [McSkimin and Andreatch, 1962; and Davies and O'Connell, this volume] tend to give systematically high values for K'.

Table 2 shows the ultrasonic results for K_T and K_T' and also gives K_T' values obtained by fitting (1) to the isotherms of McQueen et al. [1970] and assuming the ultrasonic K_T values. The fourth column shows the percentage difference between the two K_T' values. The differences are somewhat larger than rough estimates of the maximum errors ($\sim$ 5%) in the ultrasonic measurements. These errors may well have been underestimated, but it is also possible that some of the difference is due to faulty assumptions in deriving the shock isotherms from the Hugoniots, or to neglect of higher order terms in (1).

In this connection it is interesting to digress briefly by noting that the differences in Table 2 are greater for Mo and W than for Nb and Ta. In Figure 10, the shock Hugoniots in fact lie about halfway in between the ultrasonic and shock isotherms, whereas in Figure 9 they fall on or above the ultrasonic curves. The differences between the group VB and VIB elements cannot therefore be explained by errors in reducing

the shock compression data. It also seems unlikely that the ultrasonic measurements should be in substantially greater error for Mo and W than for Nb and Ta since all of the experimental work was carried ou by one worker using the same equipment and techniques. It thus appears that higher order effects involving $K_T'' = (\partial^2 K_T/\partial P^2)_T$ may be greater in the group VIB than in the group VB elements (i.e., $K_T K_T''$ is more negative in the former group).

Regardless of the cause of disagreement at high pressures, the shock compression and ultrasonic isotherms agree quite well at lower pressures and indeed can provide a good check on other types of experiments. With this in mind, the compression of Nb in a diamond-anvil pressure cell has been studied by the x-ray diffraction technique under both hydrostatic and nonhydrostatic conditions in order to determine the effects of nonhydrostatic stresses.

In the present study the Bassett type diamond cell [Bassett et al., 1967] was used. The hydrostatic P-V measurements were carried out up to 55 kbar by gasketing the sample immersed in a 4:1 methanol:ethanol mixture between the anvils and by using the ruby fluorescence pressure calibration method [Piermarini et al., 1973, 1975]. In addition, some hydrostatic measurements used NaCl as the pressure indicator instead of ruby. In the nonhydrostatic experiments, which extended up to 175 kbar, a fine mixture of Nb and NaCl (1:4 in volume) was gasketed between the diamond anvils without any liquid pressure medium. When

NaCl was used, the isothermal compression curve of Weaver et al. [1970] determined the pressure.

The results are shown in Figure 11, together with the direct compression measurements of Vaidya and Kennedy [1972] and the extrapolation of the ultrasonic results [Katahara et al., 1976]. In this pressure region, the shock isotherm of McQueen et al. [1970] falls very slightly below the ultrasonic curve. Equation (1) has been fitted both to the hydrostatic and to the nonhydrostatic data by a least squares procedure in which K_T' has been assumed to be equal to the ultrasonic value. The K_T values obtained are given in Table 3 and the corresponding curves are also shown in Figure 11.

Given the scatter and the limited pressure range for the hydrostatic data, about all that can be said is that they are consistent with both the ultrasonic and the shock wave measurements. On the other hand, the nonhydrostatic points tend to fall above the ultrasonic curve (and hence the shock compression curve also). In Table 3 it can be seen that the nonhydrostatic K_T is higher than the ultrasonic K_T by three standard errors.

Pressure intensification effects as suggested by Jamieson and Olinger [1968] and Sato et al. [1973] would cause lower rather than higher observed volumes for the nonhydrostatic case. The discrepancy is more likely caused by the existence of a uniaxial stress in the sample parallel to the load axis of the cell. In a study of the strain configuration of different materials in an ungasketed diamond anvil cell, Kinsland

[1974] observed that strains in NaCl were virtually isotropic up to 200 kbar. On the other hand, he found that materials with greater yield strengths such as MgO and Mg_2SiO_4 (forsterite) showed significantly higher elastic strains parallel to the load axis than perpendicular to it. This is shown schematically in Figure 12. Lattice planes parallel to the load axis have larger lattice spacings than planes perpendicular to the axis (i.e., $a_{||} > a_{\perp}$). In cases where the incident x-ray beam is parallel to the load axis, only those lattice planes with large spacings participate in the observed Bragg diffraction and the volume inferred from the assumption that $V = a_{||}^3$ is thus larger than the true volume ($V = a_{||}^2 \cdot a_{\perp}$) at the pressure indicated by the NaCl standard. On the basis of hydrostatic measurements on Fe_2SiO_4 (spinel), Wilburn [1975] concluded that this kind of effect was present in the earlier ungasketed experiments of Mao et al. [1969] on the same substance. It is not unreasonable to suppose that the yield strength of Nb is large enough to cause the present nonhydrostatic data to be similarly offset toward higher volumes. This study therefore provides further evidence that nonhydrostatic equation of state experiments can be significantly in error, especially for materials with high yield strengths and low compressibilities.

ACKNOWLEDGMENTS

We are indebted to Gary W. Shannette for the use of his Ta-W alloy crystals and for showing us his data before publication.

REFERENCES

Anderson, D.L., and R.S. Hart, An earth model based on free oscillations and body waves, J. Geophys. Res., 81, 1461-1475, 1976.

Birch, F., The effect of pressure upon the elastic properties of isotropic solids, according to Murnaghan's theory of finite strain, J. Appl. Phys., 9, 279-288, 1938.

Birch, F., Finite elastic strain of cubic crystals, Phys. Rev. 71, 809-824, 1947.

Bassett, W.A., T. Takahashi, and P.W. Stook, X-ray diffraction and optical observations on crystalline solids up to 300 kbar, Rev. Sci. Instrum., 38, 37-42, 1967.

Bukowinski, M.S.T., and L. Knopoff, Electronic structure of iron and models of the earth's core, Geophys. Res. Letters, 3, 45-48, 1976.

Bukowinski, M.S.T., and L. Knopoff, Physics and chemistry of iron and potassium at lower mantle and core pressures, in this volume.

Davies, G.F., and R.J. O'Connell, Transducer and bond phase shifts in ultrasonics, and their effect on measured pressure derivatives, in this volume.

Fisher, E.S., A review of solute effects on the elastic moduli of bcc transition metals, in The Physics of Solid Solution Strengthening, edited by E.W. Collins and H.L. Gegel, Plenum, New York, 1975.

Fisher, E.S., M.H. Manghnani, and K. Katahara, Application of hydrostatic pressure and shock wave data to theory of cohesion in metals, Rev. Phys. Chem. Jpn., 393-397, 1975.

Gilbert, F., and A.M. Dziewonski, An application of normal mode theory to the retrieval of structural parameters and source mechanisms from seismic spectra, Phil. Trans. Roy. Soc. London Ser. A, 278, 187, 1975.

Hubbell, W.C., and F.R. Brotzen, Elastic constants of niobium-molybdenum alloys in the temperature range -190 to +100°C, J. Appl. Phys., 43, 3306-3312, 1972.

Jamieson, J.C., and B. Olinger, Pressure Inhomogeneity: A possible source of error in using internal standards for pressure gages, in Accurate Characterization of the High-Pressure Environment, edited by E.C. Lloyd, N.B.S. Special Publication No. 236, 321-323, U.S. GPO, Washington, D.C., 1971.

Katahara, K.W., M.H. Manghnani, and E.S. Fisher, Pressure derivatives of the elastic moduli of niobium and tantalum, J. Appl. Phys., 47, 434-439, 1976.

Kinsland, G.L., Yield strength under confining pressures to 300 kbar in the diamond anvil cell, Ph.D. thesis, University of Rochester, Rochester, N.Y., 1974.

Mao, H.K., T. Takahashi, W.A. Bassett, J.S. Weaver, and S. Akimoto, Effect of pressure and temperature on the molar volume of wustite and of three $(Fe, Mg)_2SiO_4$ spinel solid solutions, J. Geophys. Res., 74, 1061-1069, 1969.

Mattheiss, L.F., Fermi surface in tungsten, Phys. Rev., 139, A1893-A1904, 1965.

Mattheiss, L.F., Electronic structure of niobium and tantalum, Phys. Rev. B, 1, 373-380, 1970.

McMillan, W.L., Transition temperature of strong-coupled superconductors, Phys. Rev., 167, 331-344, 1968.

McQueen, R.G., S.P. Marsh, J.W. Taylor, J.N. Fritz, and W.J. Carter, The equation of state of solids from shock wave studies, in High Velocity Impact Phenomena, edited by R. Kinslow, 293-417, Academic Press, New York, 1970.

McSkimin, H.J. and P. Andreatch, Jr., Analysis of the pulse superposition method for measuring ultrasonic wave velocities as a function of temperature and pressure, J. Acoust. Soc. Am., 34, 690-614, 1962.

Oli, B.A., and A.O.E. Animalu, Lattice dynamics of transition metals in the resonance model, Phys. Rev. B, 13, 2390-2410, 1976.

Pearson, W.B., Handbook of Lattice Spacings and Structures of Metals and Alloys, vol. 1, Pergamon, New York, 1958.

Pearson, W.B., Handbook of Lattice Spacings and Structures of Metals and Alloys, vol. 2, Pergamon, New York, 1966.

Peter, M., W. Klose, G. Adam, P. Entel, and E. Kudla, Tight-binding model for transition metal electrons-1, Helv. Phys. Acta, 47, 807-832, 1974.

Pettifor, D.G., Theory of the crystal structures of transition models, J. Phys. C, 3, 367-377, 1970.

Pickett, W.E. and P.B. Allen, Density of states of Nb and Mo using Slater-Koster Interpolation, Phys. Letters, 48A, 91-92, 1974.

Piermarini, G.J., S. Block, and J.D. Barnett, Hydrostatic limits in liquids and solids to 100 kbar, J. Appl. Phys., 44, 5377-5382, 1973.

Piermarini, G.J., S. Block, J.D. Barnett, and R.A. Forman, Calibration of the R_1 ruby fluorescence line to 195 kbar, J. Appl. Phys., 46, 2774-2780, 1975.

Posternak, M., W.B. Waeber, R. Griessen, W. Joss, W. van der Mark, and W. Wejgaard, The stress dependence of the Fermi surface of molybdenum. I. The electron lenses, J. Low Temp. Phys., 21, 47-74, 1975.

Sato, Y., S. Akimoto, and K. Inoue, Pressure intensification in the composite material, High Temp-High Press., 5, 289-297, 1973.

Smith, T.F., and T.R. Finlayson, Thermal expansion of bcc solid solution alloys in the system Zr-Nb-Mo-Re, J. Phys. F: Metal Phys., 6, 709-724, 1976.

Thomsen, L., Towards an equation of state for the lower mantle (abstract), EOS Trans. A.G.U., 56, 1063, 1975.

Thurston, R.N., Ultrasonic data and the thermodynamics of solids, Proc. I.E.E.E., 53, 1320-1336, 1965.

Vaidya, S.N., and G.C. Kennedy, Compressibility of 22 elemental solids to 45 kb, J. Phys. Chem. Sol., 33, 1377-1389, 1972.

Weaver, J.S., T. Takahashi, and W.A. Bassett, Calculation of the P-V relation for sodium chloride up to 300 kilobars at 25°C, in Accurate Characterization of the High-Pressure Environment, edited by E.C. Lloyd, N.B.S. Special Publication No. 326, 189-200, U.S. GPO, Washington, D.C., 1971.

Wilburn, R.D., Isothermal compression of spinel (Fe_2SiO_4) up to 100 kbar with the gasketed diamond cell, M.S. thesis, University of Rochester, Rochester, N.Y., 1975.

TABLE 1. Structure of Alloys Based on Transition Elements of Groups IV, V and VI

e/a Range	Structure
$4.0 < e/a < 4.1$	hcp
$4.1 < e/a < 4.2$	hexagonal (omega phase)
$4.2 < e/a < 6.3$	bcc
$6.3 < e/a$	hcp

TABLE 2. The isothermal bulk modulus, K_T, and its pressure derivative, K_T'

Element	K_T (Mbar)	K_T' Ultrasonic	K_T' Shock Wave	% Difference
Nb	1.6898	4.08	3.71	9
Ta	1.9415	3.83	3.65	5
Mo	2.6099	4.65	3.95	15
W	3.0842	4.47	3.88	13

K_T and ultrasonic K_T' values are from Katahara et al. [1976] for Nb and Ta, and from the present study for Mo and W. Shock wave K_T' were obtained by assuming the ultrasonic K_T values and fitting (1) to the isotherms of McQueen et al. [1970].

TABLE 3. Comparison of K_T and K_T' of Nb from different methods

K_T Mbar	K_T'	Equation of State Used	Experimental Method	Reference
1.690	4.08		Ultrasonic	Katahara et al. (1976)
1.71 ± 0.07	4.08*	Birch-Murnaghan	X-ray (Hydrostatic)	Present
1.79 ± 0.03	4.08*	Birch-Murnaghan	X-ray (Non-hydrostatic)	Present

*Assumed.

FIGURE CAPTIONS

Figure 1 Adiabatic single crystal elastic moduli of Nb-Mo alloys vs. e/a from present work and from Hubbell and Brotzen [1971]. K_S is the adiabatic bulk modulus, $C_L = (C_{11} + C_{12})/2 + C_{44}$, and $C' = (C_{11} - C_{12})/2$.

Figure 2 Adiabatic single crystal elastic moduli of Ta-W alloys vs. e/a from present work and from Shannette [personal communication].

Figure 3 Pressure derivatives of the elastic moduli of Nb-Mo alloys vs. e/a.

Figure 4 Pressure derivatives of the elastic moduli of Ta-W alloys vs. e/a.

Figure 5 π_{ij} vs. e/a for Nb-Mo alloys. See text for definition of π_{ij}.

Figure 6 π_{ij} vs. e/a for Ta-W alloys.

Figure 7 ℓn A and d ℓn A/d ℓn V vs. e/a for Nb-Mo and Ta-W alloys. $A \equiv C_{44}/C'$.

Figure 8 Electronic energy bands along [100] in the Brillouin zone for bcc transition metals, after Mattheiss [1965]. Γ is the zone center and H is a corner. The dashed lines indicate the approximate positions of the Fermi energy at e/a = 5 and 6. The bands are shown without spin-orbit splitting on the left and with spin-orbit splitting on the right.

Figure 9 V/V_o vs. P/K_T for Nb and Ta. The ultrasonic curves are from Katahara et al. [1976]. The shock Hugoniots and isotherms are from McQueen et al. [1970]. The ultrasonic K_T values in Table 2 were used to normalize the pressures.

Figure 10 V/V_o vs. P/K_T for Mo and W. The ultrasonic curves are from the present results. The shock Hugoniots are from McQueen et al. [1970]. As in Figure 9 the pressures have been divided by the ultrasonic K_T values given in Table 2.

Figure 11 V/V_o vs. pressure for Nb. Open and solid circles are diamond anvil x-ray data for hydrostatic and nonhydrostatic conditions respectively. Solid lines are equation (1) with K_T and K_T' as given in Table 3. For the x-ray data, $K_T' = 4.08$ has been assumed from the ultrasonic results and K_T has been obtained from a least squares fit.

Figure 12 Schematic diagram of anisotropic strain in the diamond anvil cell after Kinsland [1974]. A circle in the unstressed sample is compressed into an ellipse. Lattice planes which are nearly parallel to the x-ray beam have larger lattice spacings than the planes which are more nearly perpendicular to the beam. Because of a limited aperture for observing diffracted x-rays, the larger lattice spacings are the ones seen experimentally and the calculated volumes are thus too large.

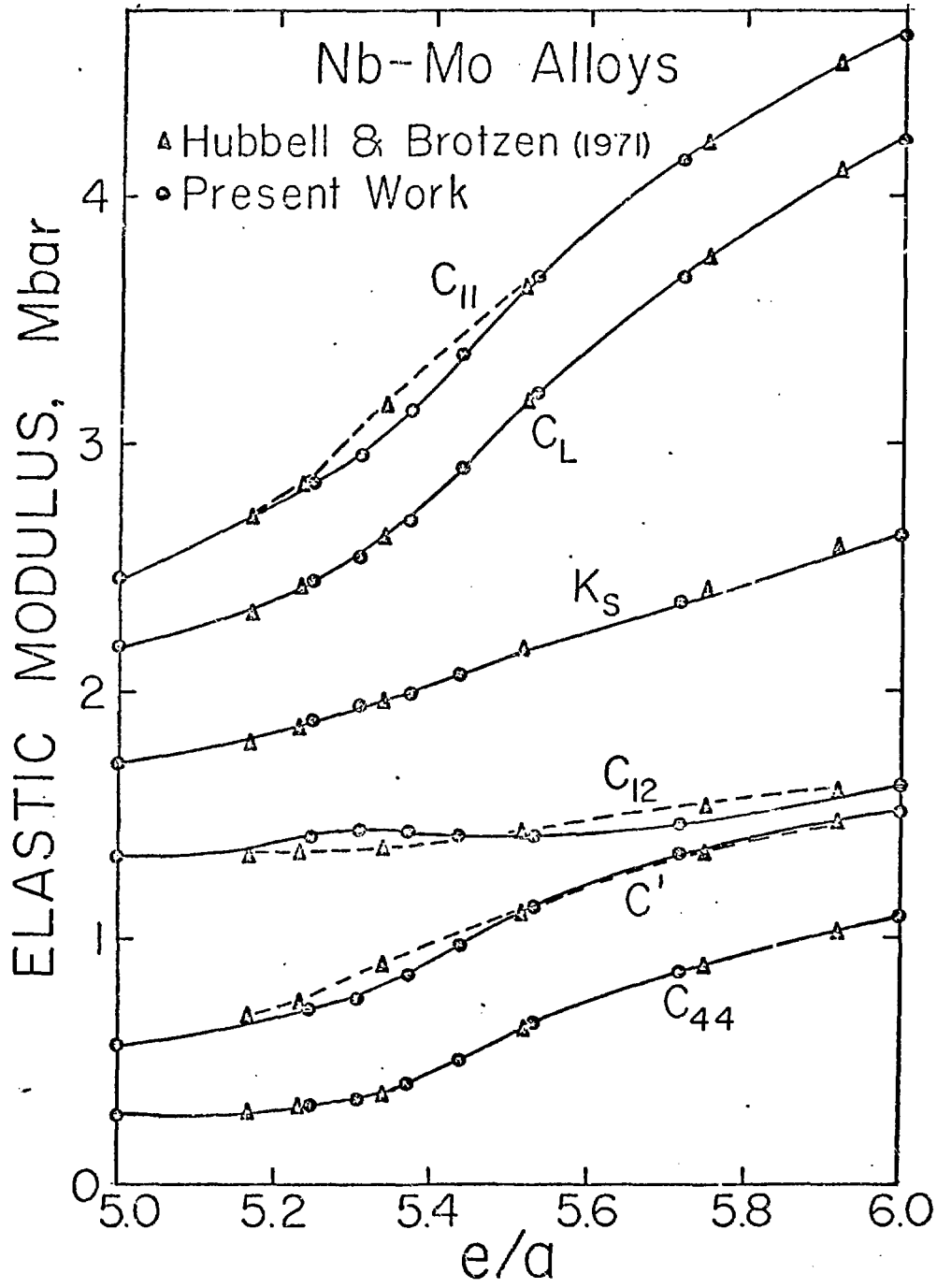
Nb-Mo Alloys
Hubbell & Brotzen (1971)
Present Work
C_{11}
C_L
K_S
C_{12}
C'
C_{44}
ELASTIC MODULUS, Mbar
0
1
2
3
4
5.0
5.2
5.4
5.6
5.8
6.0
e/a

Fig. 1

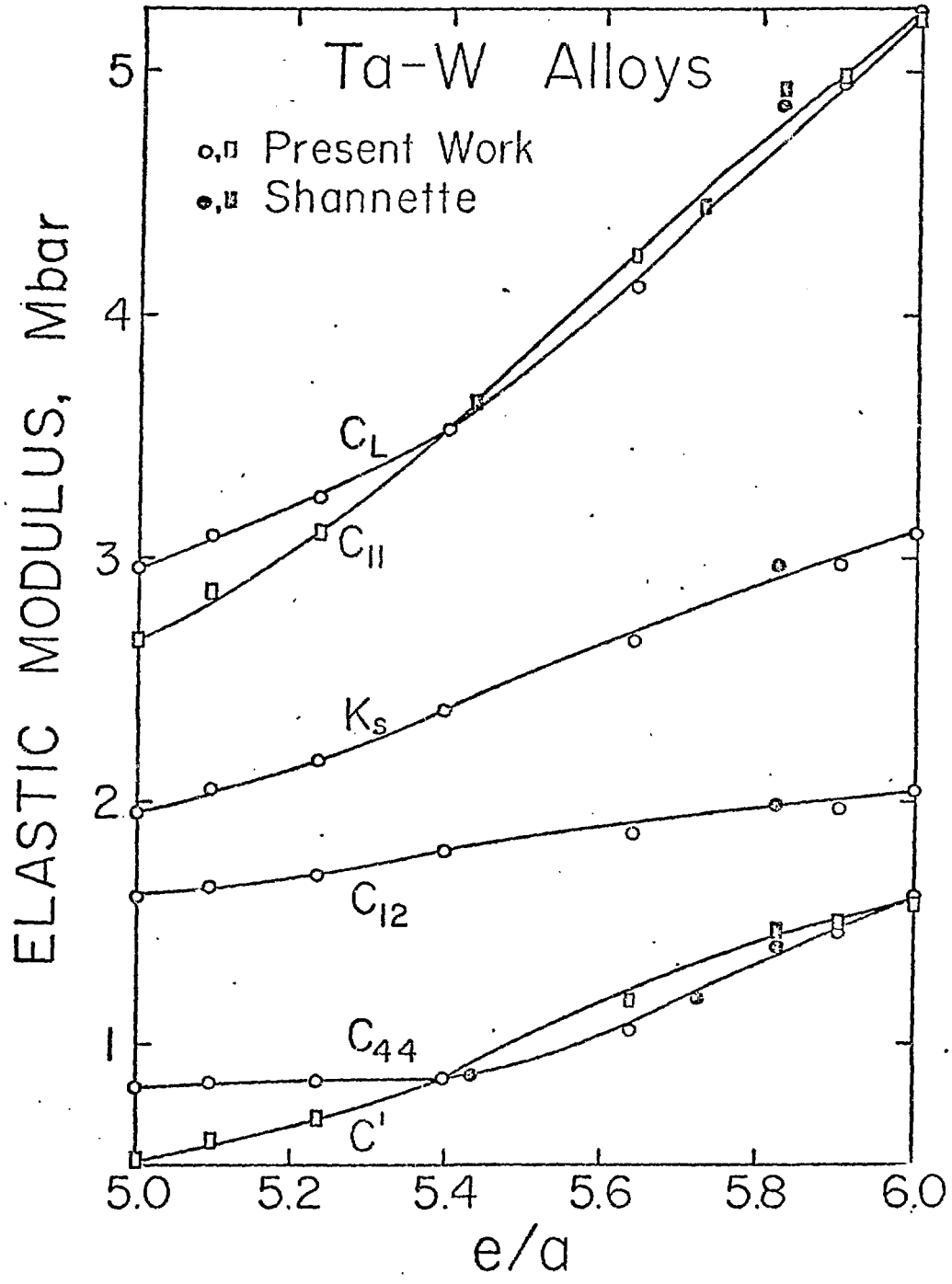
Ta-W Alloys
Present Work
Shannette
ELASTIC MODULUS, Mbar
e/a
C_L
C_{11}
K_S
C_{12}
C_{44}
C'
1
2
3
4
5
5.0
5.2
5.4
5.6
5.8
6.0

Fig. 2

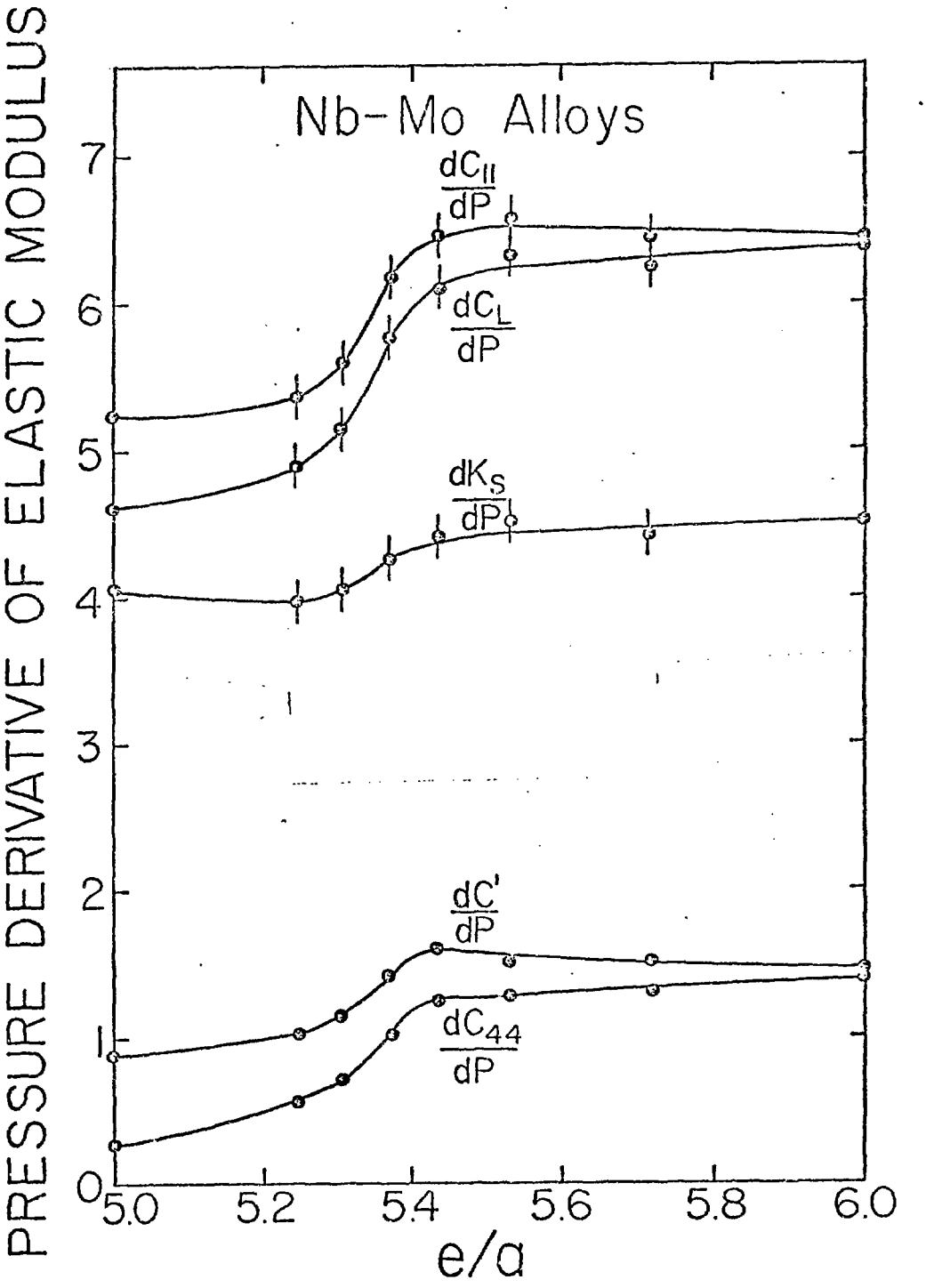
Nb-Mo Alloys
PRESSURE DERIVATIVE OF ELASTIC MODULUS
dC11/dP
dCL/dP
dKS/dP
dC'/dP
dC44/dP
0
1
2
3
4
5
6
7
5.0
5.2
5.4
5.6
5.8
6.0
e/a

Fig. 3

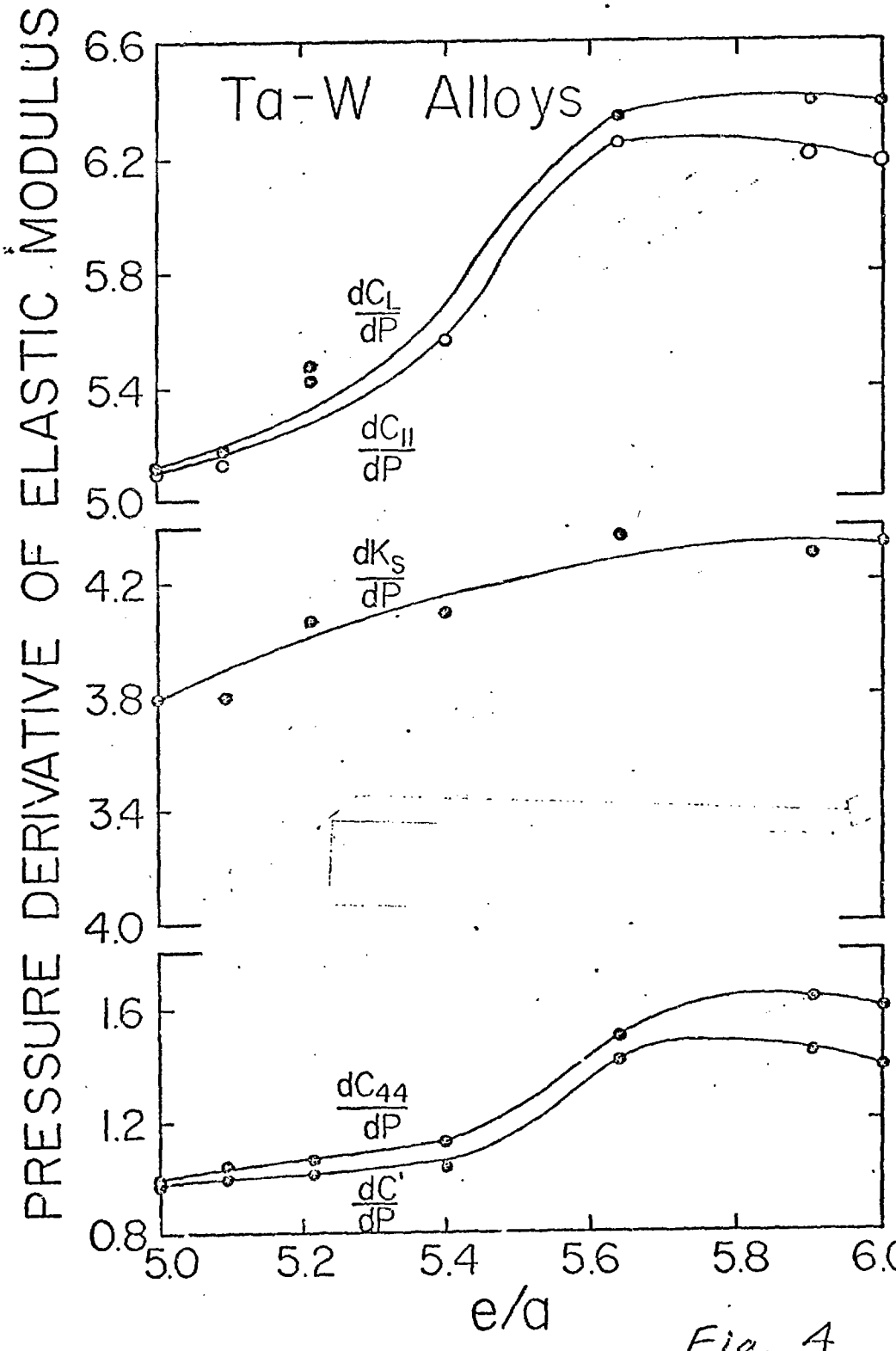
Ta-W Alloys
PRESSURE DERIVATIVE OF ELASTIC MODULUS
6.6
6.2
5.8
5.4
5.0
4.2
3.8
3.4
4.0
1.6
1.2
0.8
dC_L/dP
dC_II/dP
dK_S/dP
dC44/dP
dC'/dP
5.0
5.2
5.4
5.6
5.8
6.0
e/a

Fig. 4

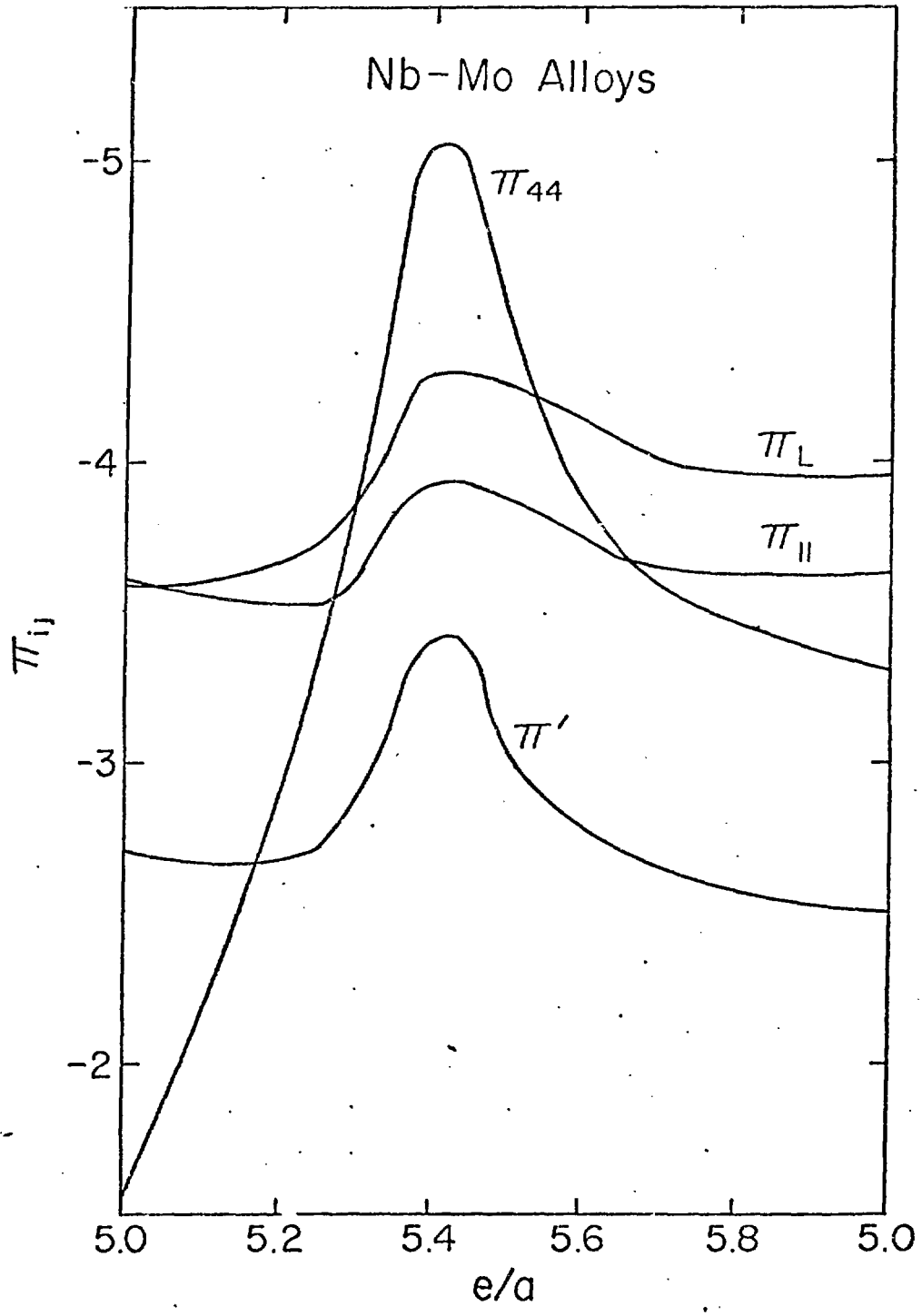

Fig. 5

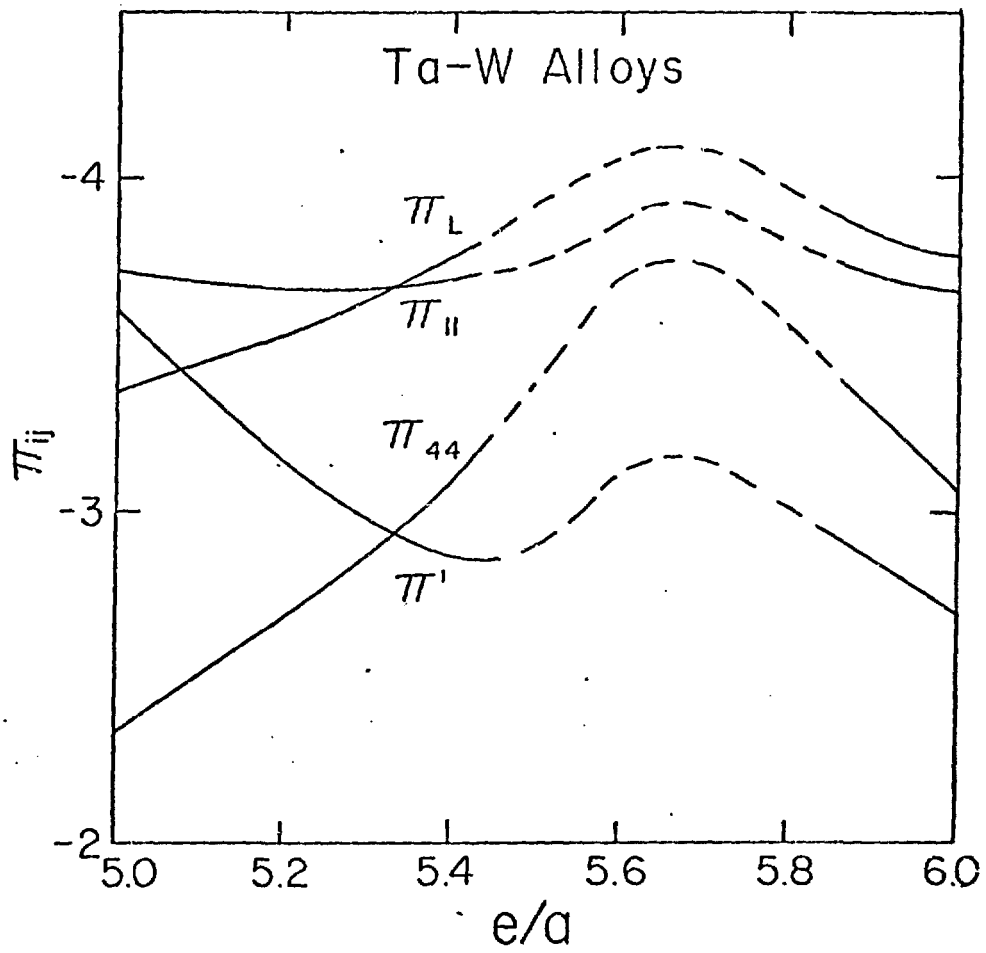

Fig. 6

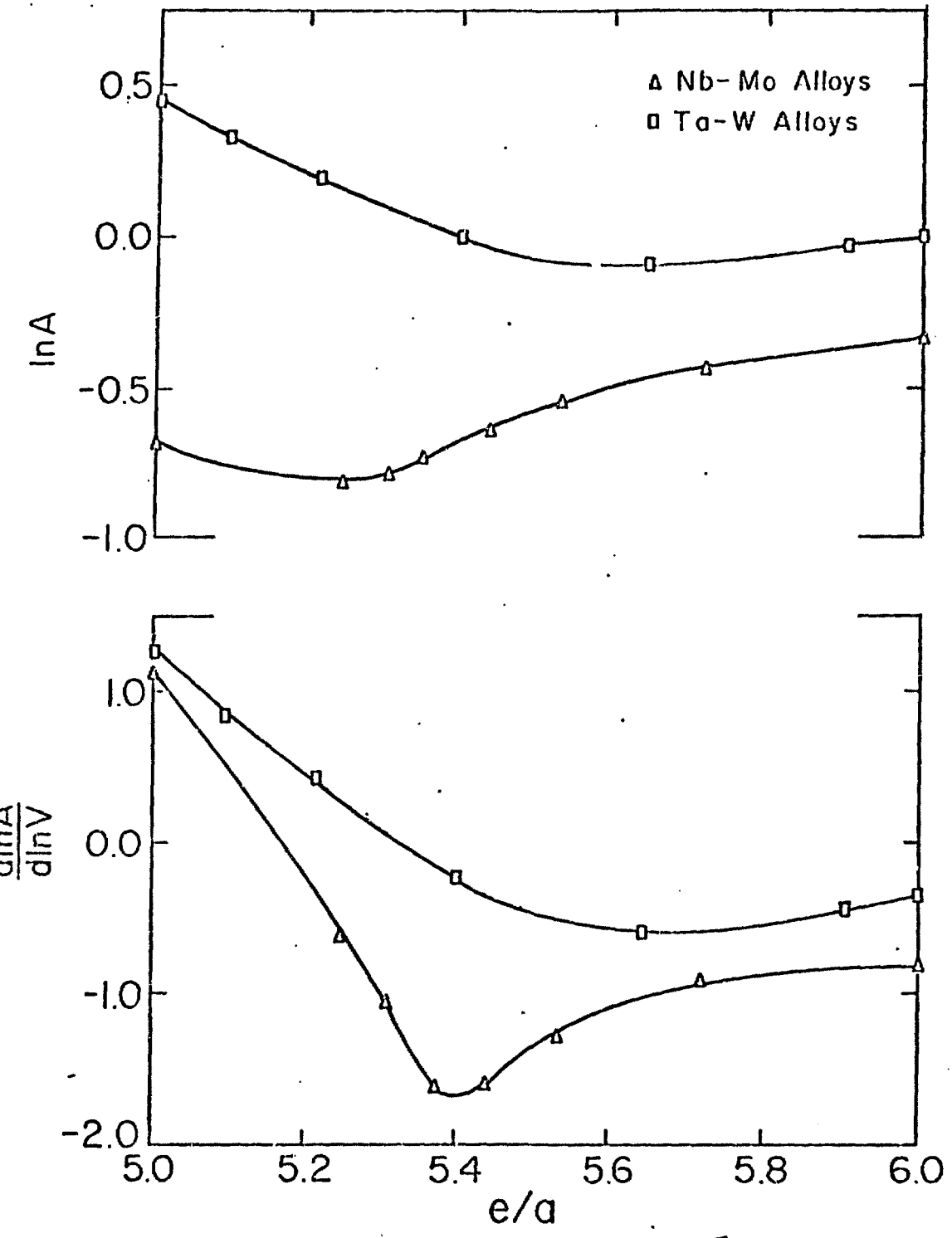
Δ Nb-Mo Alloys
□ Ta-W Alloys
0.5
0.0
-0.5
-1.0
lnA
1.0
0.0
-1.0
-2.0
dlnA/dlnV
5.0
5.2
5.4
5.6
5.8
6.0
e/a

Fig. 7

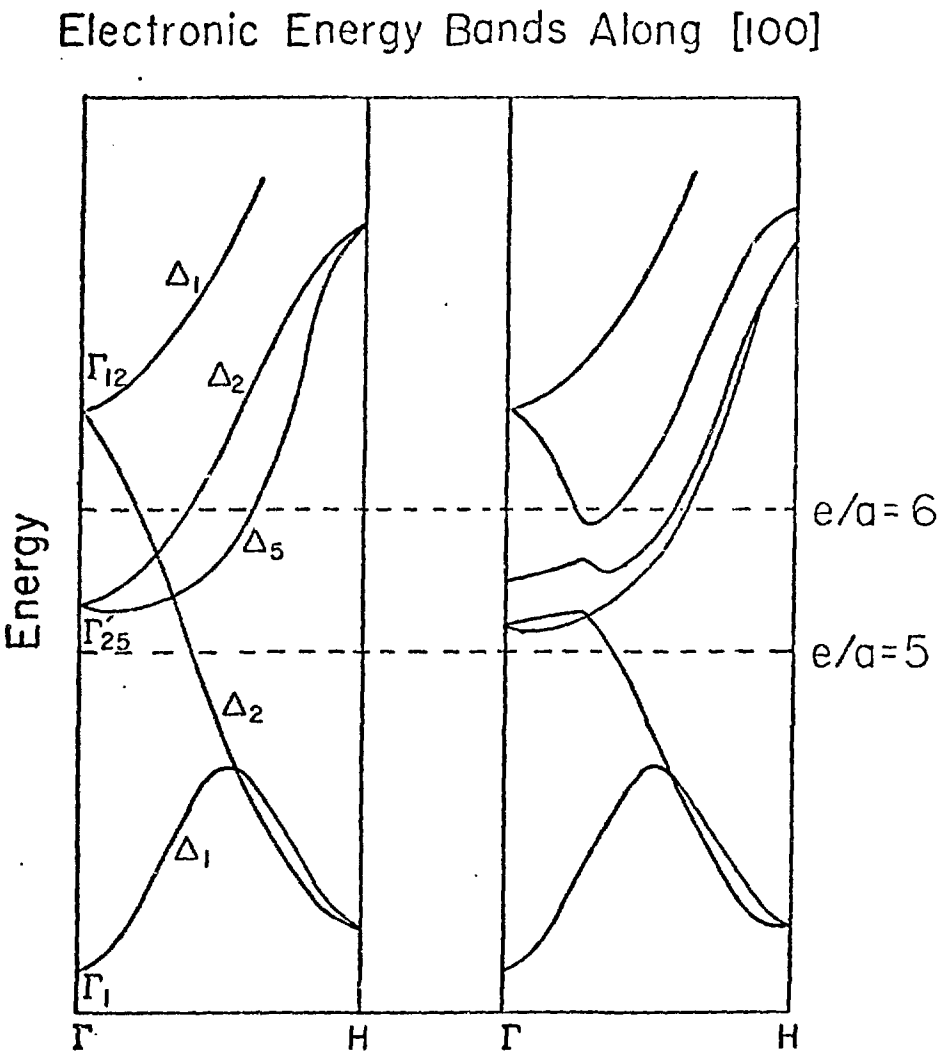
Electronic Energy Bands Along [100]
Energy
Δ1
Γ12
Δ2
Δ5
Γ'25
Δ2
Δ1
Γ1
e/a=6
e/a=5
Γ
H
Γ
H

Fig. 8

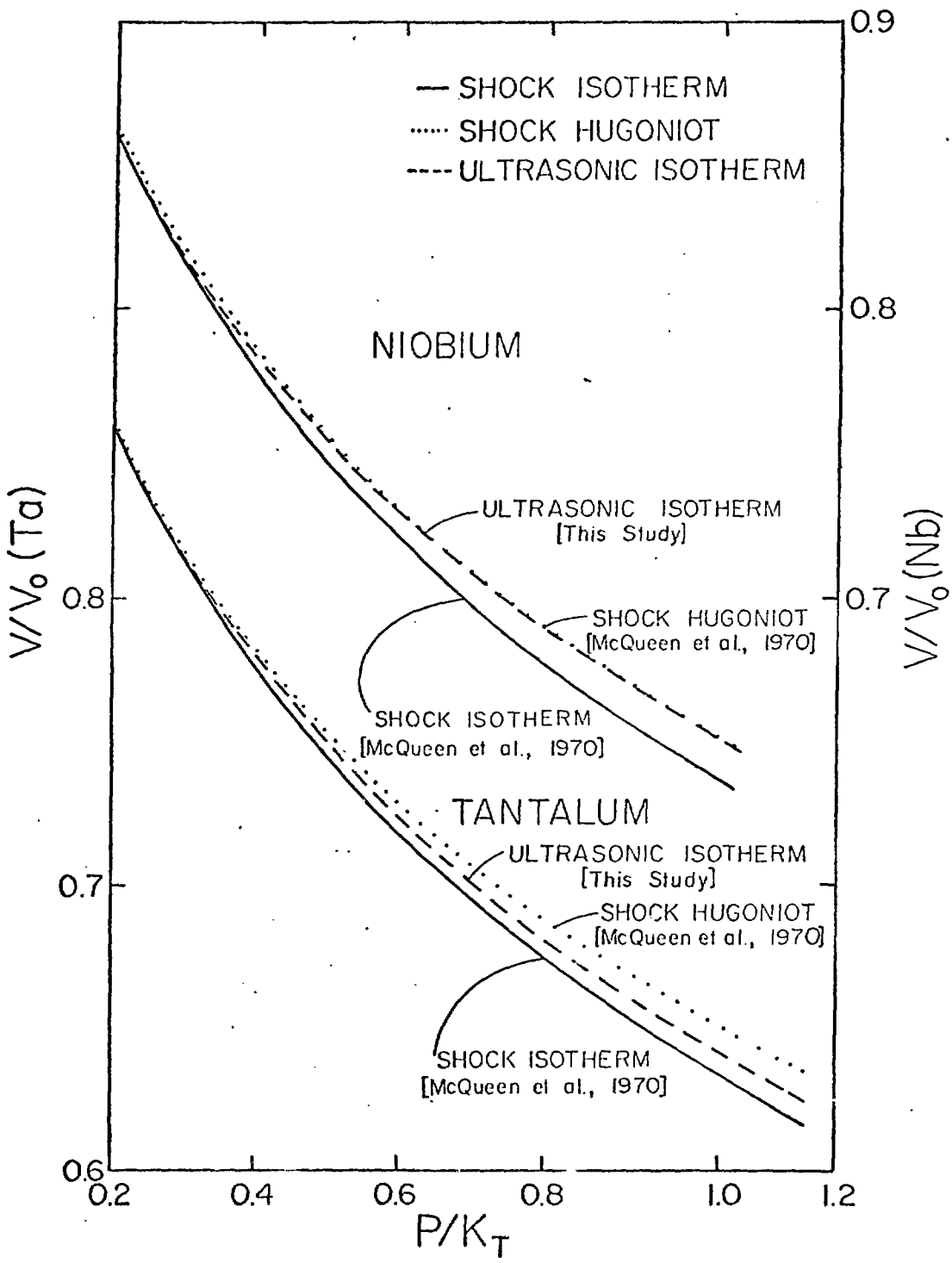
SHOCK ISOTHERM
SHOCK HUGONIOT
ULTRASONIC ISOTHERM
NIOBIUM
ULTRASONIC ISOTHERM
[This Study]
SHOCK HUGONIOT
[McQueen et al., 1970]
SHOCK ISOTHERM
[McQueen et al., 1970]
TANTALUM
ULTRASONIC ISOTHERM
[This Study]
SHOCK HUGONIOT
[McQueen et al., 1970]
SHOCK ISOTHERM
[McQueen et al., 1970]
V/V₀ (Ta)
V/V₀ (Nb)
P/K_T
0.6
0.7
0.8
0.9
0.2
0.4
0.6
0.8
1.0
1.2

Fig 9

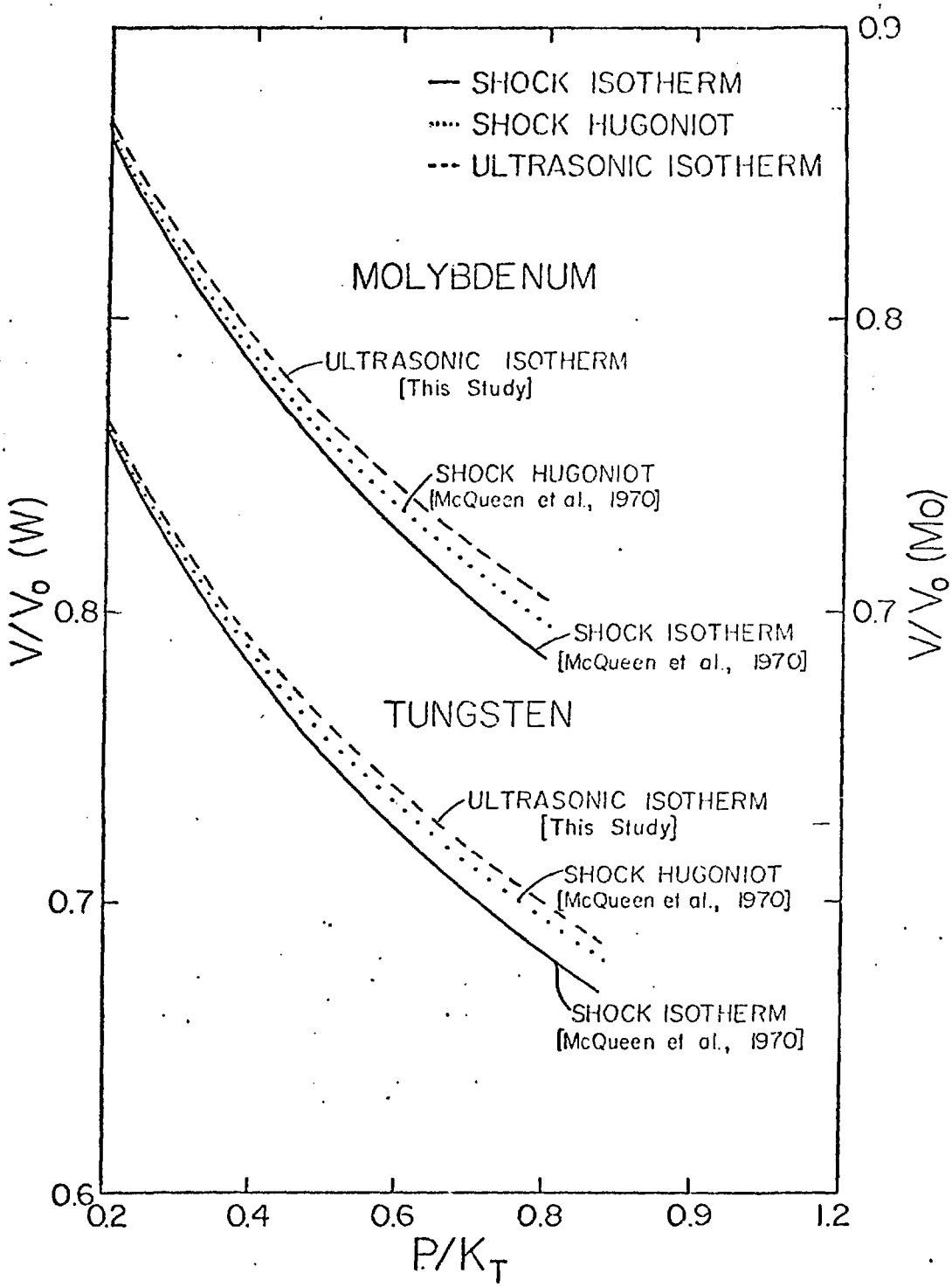
— SHOCK ISOTHERM
····· SHOCK HUGONIOT
--- ULTRASONIC ISOTHERM
MOLYBDENUM
ULTRASONIC ISOTHERM
[This Study]
SHOCK HUGONIOT
[McQueen et al., 1970]
SHOCK ISOTHERM
[McQueen et al., 1970]
TUNGSTEN
ULTRASONIC ISOTHERM
[This Study]
SHOCK HUGONIOT
[McQueen et al., 1970]
SHOCK ISOTHERM
[McQueen et al., 1970]
V/V₀ (W)
V/V₀ (Mo)
P/K_T
0.6
0.7
0.8
0.9
0.2
0.4
0.6
0.8
0.9
1.2

Fig. 10

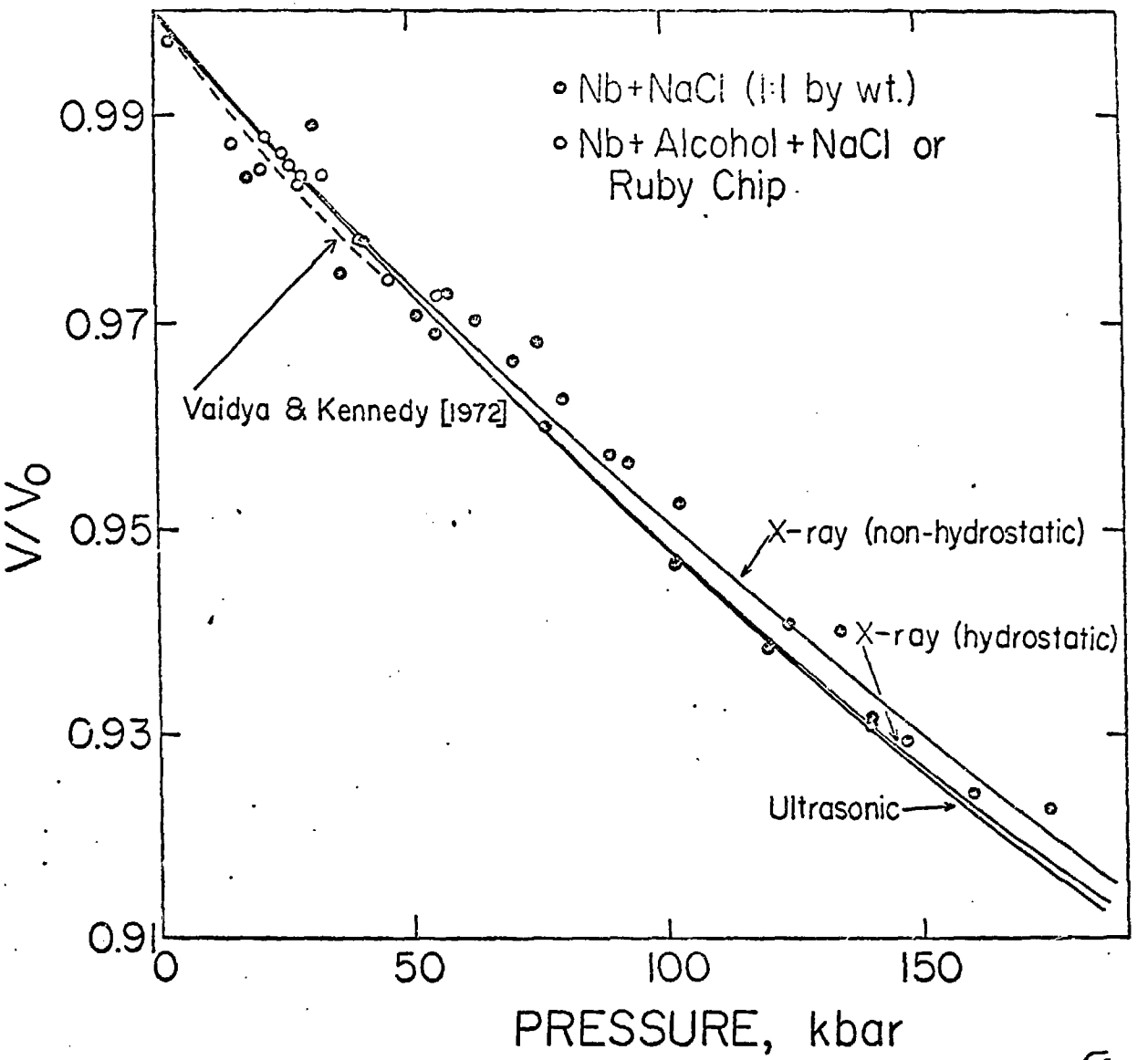
Nb+NaCl (1:1 by wt.)
Nb+Alcohol+NaCl or Ruby Chip
Vaidya & Kennedy [1972]
X-ray (non-hydrostatic)
X-ray (hydrostatic)
Ultrasonic
V/V0
0.99
0.97
0.95
0.93
0.91
0
50
100
150
PRESSURE, kbar

Fig. 11

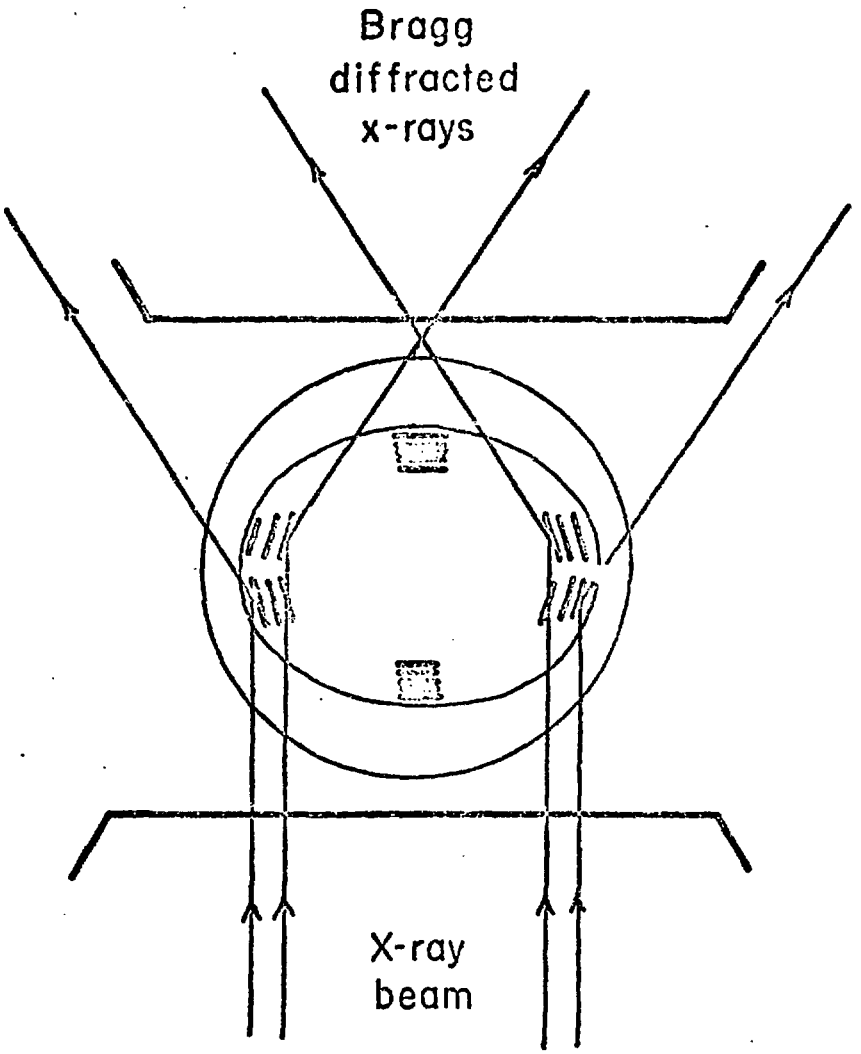

[Kinsland, 1974]

Fig. 12